

Radio galaxies in cooling core clusters. Restarted activity in the nucleus of 3C 317?

T. Venturi¹, D. Dallacasa^{1,2}, and F. Stefanachi¹

¹ Istituto di Radioastronomia del CNR, Via Gobetti 101, 4129 Bologna, Italy

² Dipartimento di Astronomia, Via Ranzani 1, 40127 Bologna, Italy

Received November 17, 2018; accepted ?

Abstract. We present the results of VLBA observations of the radio galaxy 3C 317, associated with the cD galaxy UGC 09799 at the centre of the cooling core cluster of galaxies A2052.

These observations were carried out at 1.7 GHz, 4.9 GHz and 8.3 GHz, in polarimetric mode, and allowed us to image the parsec scale region of the source. Our analysis suggests that the nucleus of 3C 317 hosts a very young radio source. The estimated radiative age for the radio structure within the inner 10 pc is ~ 170 yr. Given the existence of extended radio emission on the arcsecond scale, we suggest that 3C 317 is a restarted radio galaxy. The implications of this result in the light of the interaction between radio plasma and thermal hot gas in clusters of galaxies are briefly discussed.

Key words. cooling flows - galaxies: clusters: individual(Abell2052) - galaxies: nuclei - galaxies: structure - radio continuum:galaxies

1. The current knowledge of 3C317 properties

The radio galaxy 3C 317 ($RA_{J2000} = 15^h 16^m 44.5^s$, $DEC_{J2000} = 07^\circ 01' 17''$, redshift $z = 0.035$) is associated with the cD galaxy UGC9799, located at the centre of the cooling core cluster of galaxies A2052.

With a total power $P_{tot}(1.4 \text{ GHz}) = 5.4 \times 10^{24} \text{ W Hz}^{-1}$, and a core power $P_{core}(5 \text{ GHz}) = 2.2 \times 10^{24} \text{ W Hz}^{-1}$, the radio galaxy falls in the range of low luminosity radio galaxies¹. Unlike the typical Faranoff–Riley Type I radio sources (FRI, Fanaroff & Riley 1974), characterized by core, twin jets and lobes, 3C 317 shows an amorphous halo surrounding a bright core, coincident with the optical centre of the galaxy. This core–halo structure is common among the steep spectrum compact cores in radio sources associated with the central galaxies in cooling core clusters (Burns 1990).

While the connection between amorphous steep spectrum radio galaxies and cooling clusters is an established phenomenon, their causal link is still unclear. Radio studies of central cluster galaxies (O’Dea & Baum 1987; Burns 1990; Taylor et al. 1994) show that cooling clusters may host both extended twin–jet radio galaxies and amorphous sources, however radio galaxies of this latter class

are found exclusively in a cooling cluster environment. Examples of cooling clusters with an extended central radio galaxy are A2029, A4059 (Taylor et al. 1994), A2199 (Ge & Owen 1993), Hydra A (Taylor & Perley 1993); compact radio galaxies similar to 3C 317 are 3C 84 in the Perseus cluster (Böhringer et al. 1993), PKS 0745–191 (Baum & O’Dea 1991), 2A 0335+096 (Sarazin et al. 1995). Baum & O’Dea (1991) and Sarazin et al. (1995) discussed possible forms of interaction between the radio sources and the cooling flow, i.e. disruption of the radio jets by the high–pressure ambient gas, buoyant effects on the amorphous radio emission, cooling gas as power supplier for the central radio galaxy, and finally gas heating in the inner cluster region from the central radio galaxy. More recently, thanks to the high resolution imaging capabilities of the X–ray satellite Chandra, the interaction between the radio plasma and the hot gas in cooling clusters has become even clearer, and it is now accepted that the intracluster gas and the central radio galaxy mutually influence each other. Examples include Hydra A (McNamara et al. 2000; David et al. 2001), and Perseus (Fabian et al. 2000). In both cases, there is an anticoincidence between the radio and X–ray emission. In particular, the radio lobes on scales of tens (or hundreds) of kpc are located in “holes” of the X–ray emission.

Major interaction between the radio plasma and the intracluster gas is now established also in the case of 3C 317. Comparison between arcsecond radio images and Chandra

Send offprint requests to: tventuri@ira.cnr.it

¹ We will use $H_0 = 50 \text{ km s}^{-1} \text{ Mpc}^{-1}$, $q_0 = 0$ and $S \propto \nu^{-\alpha}$ throughout the paper. For 3C 317 $1 \text{ mas} \sim 1 \text{ pc}$. We define $h = H_0/100$

images suggests that the radio source has swept the gas away from the centre of the cluster, compressing it into bright shells surrounding two “holes” in the X-ray emission (Blanton et al. 2001; Rizza et al. 2000).

3C 317 was studied in detail with the Very Large Array (VLA) at arcsecond resolution at 90, 20, 6 and 3.6 cm (Zhao et al. 1993). It is characterized by a compact core and bipolar radio emission oriented in the North-South direction. This radio emission is embedded in an amorphous halo, which shows considerable substructure at high resolution. The integrated spectrum over the range 0.01 – 8 GHz shows a break around 0.5 GHz, and it is well fitted by two power laws with $\alpha = 1.4$ for $\nu > 0.5$ GHz and $\alpha = 0.8$ for $\nu < 0.5$ GHz. These spectral features and the radio morphology suggest that diffusion, synchrotron losses and electron reacceleration are important in this radio halo. Another peculiar property is the high integrated rotation measure, $RM \sim -800 \text{ rad m}^{-2}$ (Taylor et al. 1992). High RMs are common in radio galaxies at the centre of cooling core clusters, and they are usually explained as due to a magnetized external screen (Ge & Owen 1994).

At milliarcsecond resolution the source shows a bent morphology, and the radio emission on this scale has a flat spectrum up to 5 GHz (Venturi et al. 2000). This suggests that the subarcsecond core is active now, and raises the problem of its relation to the amorphous steep spectrum halo.

In order to study the polarimetric properties of 3C 317 on the parsec scale, and to address the issue of the connection between the parsec and kiloparsec scale components of the radio emission, we performed a multifrequency polarimetric study with the Very Long Baseline Array (VLBA). Our results are presented in this paper, which is organised as follows. In §2 we describe the radio observations and data reduction; the images are presented in §3 and are analysed in §4; the results are discussed in §5; conclusions are given in §5.

2. Observations

3C317 was observed on March 5, 1999 using the full VLBA array, one VLA antenna and the Effelsberg antenna, simultaneously at 1.7 GHz (L band), 4.9 GHz (C band) and 8.3 GHz (X band), in polarimetric mode. The total allocated time (9 hours) was equally split among the three bands. The 4.9 and 8.3 GHz observations were carried out using two well separated sub-bands of 8 MHz each, in order to optimise the u–v coverage and to derive the Rotation Measure with four points. Details of the observations are given in Table 1, where for each band we report the bandwidth, the observing frequencies (ν_{IF1} and ν_{IF2}), the total time on source, the minimum and maximum baseline.

The data were correlated at the VLBA correlator in Socorro (New Mexico). Standard a-priori calibration, self-calibration, imaging and analysis were carried out using the NRAO Astronomical Image Processing System

(AIPS). The accuracy of the absolute flux density scale is of the order of $\sim 4 - 5 \%$ at all frequencies.

Polarisation calibration and imaging were performed at 4.9 GHz and 8.3 GHz following the general method described in Cotton (1993), and implemented into AIPS by means of a number of procedures. No polarisation imaging was performed at L band. Instrumental polarisation corrections were determined from measurements of 0016+731, known to be unpolarised, while observations of 3C286 were used to derive absolute polarisation position angle χ . We used the sum of the Q and U CLEAN components obtained from a subset of short baselines, and compared our results with Jiang et al. (1996). The accuracy of the absolute orientation of χ is estimated of the order of $2^\circ - 3^\circ$ at both C and X bands. For our analysis, we imaged the IF1 and IF2, for the Q and U components, separately.

3. Parsec scale morphology

3.1. Total intensity images

The uniform weighted total intensity images of 3C 317 at 1.7, 4.9 and 8.3 GHz are shown in Figs. 1, 2 and 3 respectively, while in Table 2 we give the main parameters of the same images. In particular for each band we report the total flux density, the peak flux density, the r.m.s. noise and the restoring beam. The source is characterised by an overall symmetric structure, with a centre of activity and two opposing jets with twisted morphology. The brightness asymmetry in the jets and the details of the twisting change with frequency and resolution.

At 1.7 GHz (Fig. 1) the source is dominated by a barely resolved central component, with two faint jets, elongated roughly in the N–S direction, whose surface brightness decreases quite smoothly. The two jets are slightly asymmetric, the northern being longer and brighter than the southern one. The overall position angle is $\sim -5^\circ$. The morphology of 3C 317 in this image resembles the bipolar structure of Zhao et al. (1993). Hereinafter, we will refer to the jets on this scale as the bipolar emission.

The higher resolution of the 4.9 GHz image (Fig. 2) allows us to resolve the 1.7 GHz central feature. The source has a symmetric structure, with a compact component, which includes the core of the radio emission, and two short jets, bending at ~ 5 mas from the peak, in a S-shaped structure. The overall position angle is $\sim -20^\circ$. At distance greater than 10 mas from the peak we find positive residuals on both sides, aligned in the North–South direction, which we interpret as hints of the faint symmetric jets revealed at 1.7 GHz, resolved out in this image.

At 8.3 GHz the S-shaped morphology of 3C 317 is even more pronounced. Two very short jets (see Fig. 3) are aligned at $\sim -32^\circ$ with respect to the compact component (C). They lose their collimation within the first few mas, to form two features (N and S) which slightly bend counterclockwise, and give the source a “twisted” mor-

Table 1. Parameters of the observations

Band	Bandwidth MHz	ν_{IF1} GHz	ν_{IF2} GHz	t hr	U_{min} $M\lambda$	U_{max} $M\lambda$
L	8+8	1.658	1.667	2.30	0.15	48
C	8+8	4.860	4.995	2.30	0.44	142
X	8+8	8.213	8.421	2.30	0.73	283

phology. These northern and southern features are very similar in shape, size and flux density. In particular, the ratios between their flux density, major and minor axes are respectively 1.5, 1.4 and 1.3. We note that the southern structure S is longer and brighter than the northern one. This is opposite to what is found at 1.7 GHz on the scale of tens of mas, where the northern jet is more prominent than the southern. The overall source structure at this frequency is still elongated roughly in the N–S direction, with a position angle of -22.5° . At this frequency and resolution the faint jets revealed at 1.7 GHz are completely lost.

We are aware of the fact that the images presented here differ from those (EVN and MERLIN) published in Venturi et al. (2000). The details of both sets of images can be accounted for by the different u–v coverage, resolution and sensitivity. Moreover, the combination of the EVN and MERLIN observations, may have resulted in residual amplitude errors, affecting the reliability of the images. Despite the much better quality of the present observations and the different spatial regions sampled in the source, however, we note that the orientation of the inner parsec-scale structure is in reasonable agreement with the older datasets.

As a general comment, a remarkable feature of the overall structure of 3C317 is the change of the position angle, which smoothly rotates by $\sim 20^\circ - 25^\circ$ going from the bipolar low brightness jets detected at 1.7 GHz on a scale of 20 – 40 mas (corresponding to a linear scale of 20 to 40 pc) to the inner symmetric structure detected at 8.3 GHz within 5 mas from the central compact component (~ 5 pc). It is noteworthy that the length and brightness asymmetry of the morphology changes from 1.7 GHz to the inner mas imaged at 8.3 GHz. All these details reflect the complexity of the source on all scales. Even though the overall orientation of the structure embedded in the radio halo is the North – South direction, details and fine structure change considerably depending on the frequency and resolution (Zhao et al. 1993; Ge & Owen 1994; Venturi et al. 2000).

The flux density ratio between the northern and southern jet components, as derived from the 8.3 GHz image, i.e. $R = S_S/S_N = 1.5$, gives us some information on the source orientation in the plane of the sky. Assuming that any brightness asymmetry is due to Doppler boosting in an intrinsically symmetric source, $R = 1.5$ implies $\beta \cos \theta \sim 0.08$, where β is the intrinsic speed of the relativistic plasma and θ is the viewing angle. Such con-

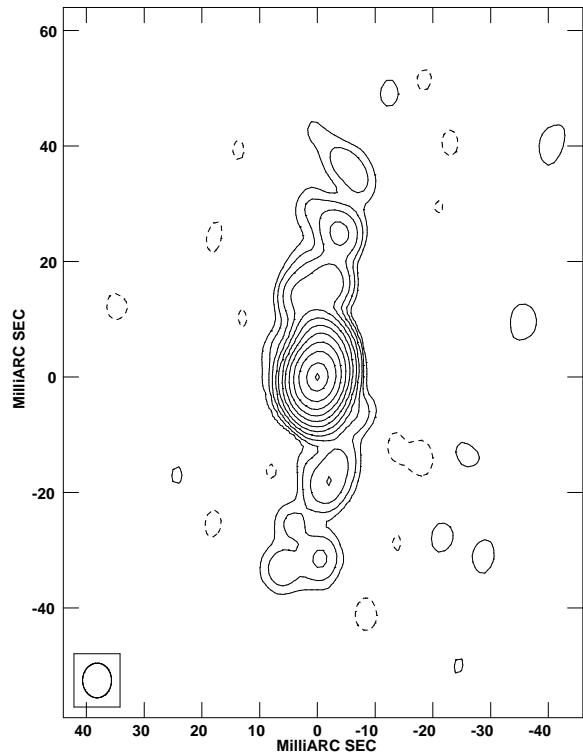


Fig. 1. 1.7 GHz image of 3C317. Peak: 276 mJy/beam. Contours: $0.19 \times (-1, 1, 2, 4, 8, 16, 32, 64, 125, 250, 500, 1000, 1400)$ mJy/beam. Restoring beam FWHM: 6×5 (mas) at 0° .

straint gives very large angles to the line of sight even for a mildly relativistic bulk motion of the radio plasma, i.e. $\theta(\beta = 1) \sim 85^\circ$, and $\theta(\beta = 0.5) \sim 81^\circ$.

3.2. Polarisation properties

The arcsecond scale core of 3C317 is known to be unpolarised (Ge & Owen 1994). The possibility of beam depolarisation is ruled out by our observations: we did not manage to reveal any polarised emission from 3C317 either at C or at X band. In particular at X band, where we had the best combination of sensitivity and resolution, we can exclude any polarised emission stronger than 0.3 mJy/beam at the full resolution of the observations. In the polarised emission images at 8.2 and 8.4 GHz, after correction for

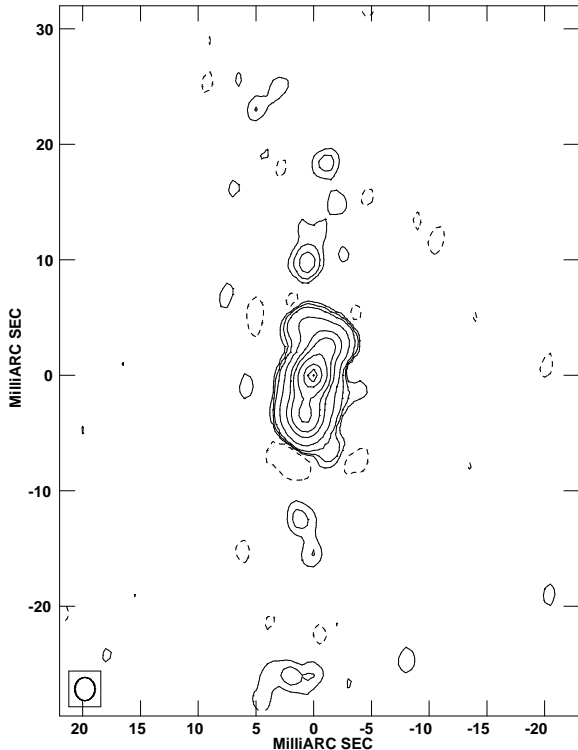


Fig. 2. 4.9 GHz image of 3C317. Peak: 155 mJy/beam. Contours: $0.19 \times (-1, 1, 2, 4, 16, 64, 125, 250, 500, 700, 800)$ mJ/beam. Restoring beam FWHM: 2×1.73 (mas) at 0° .

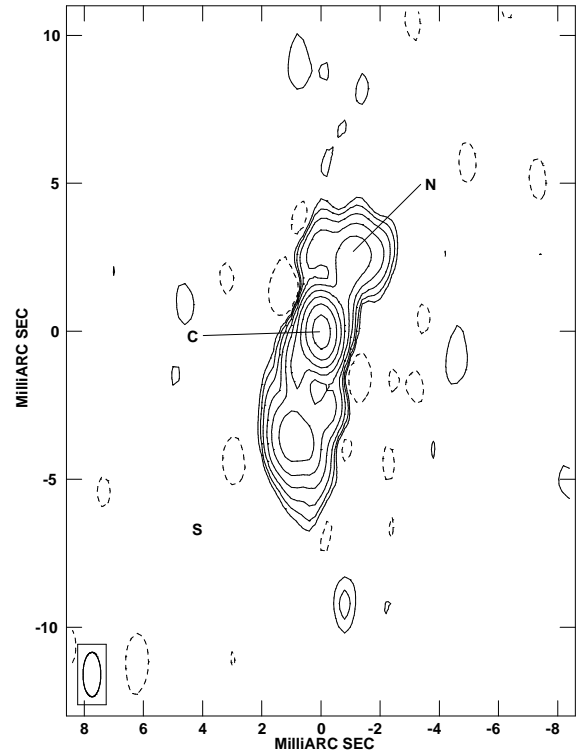


Fig. 3. 8.3 GHz image of 3C317. Peak: 102 mJy/beam. Contours: $0.27 \times (-1, 1, 2, 4, 8, 16, 32, 64, 125, 250, 400)$ mJy/beam. Restoring beam FWHM: 1.5×0.6 (mas) at 0° .

the rician bias, the r.m.s. noise is ~ 0.06 mJy/beam. The very few 5σ peaks (mostly off-source) happen at different locations at the two frequencies. Therefore, either the source is completely unpolarised on the pc scale or the Faraday screen is not resolved by the present observations. We can set conservative upper limits to the fractional peak polarisation from the jets to 10% for the northern one and to 5% for the brighter southern one. The core is at most 0.3% polarised. We obtained even more stringent upper limits (4%, 2% and 0.2% respectively) from the C band data, but we must consider that the lower resolution does not allow to disentangle possible structure in the polarised signal among the three main components partly blended together.

4. Parsec scale properties

4.1. The parsec scale spectrum

We used our multifrequency data to determine the spectral index on the parsec scale structure between 1.7 and 4.9 GHz, and between 4.9 and 8.3 GHz. For our analysis we made images of the source using the same maximum and minimum baseline in the $u-v$ coverage, the same gridding and the same restoring beam.

Between 1.7 and 4.9 GHz the $u-v$ cut applied to our datasets allowed us to determine only the total spectral index of the brightest component in the 1.7 GHz image (Fig. 1), given that the resolved emission seen at 1.7 GHz is barely detected at 4.9 GHz and the structure seen in this latter image is almost unresolved in the former. Our images were fitted with a gaussian component, whose dimensions are 4×1 mas. The spectral index is $\alpha_{1.7}^{4.9} \sim -0.01_{-0.09}^{+0.10}$, in perfect agreement with the values derived in the previous work of Venturi et al. (2000) and Zhao et al. (1993).

In order to derive an estimate of the spectral index in the bipolar milliarcsecond jets visible at 1.7 GHz, we made a naturally weighted 4.9 GHz image, and convolved it with the full resolution 1.7 GHz restoring beam. We are aware of the different coverage at the short baselines introduced by this procedure, however our approach is justified by the fact that the full resolution 4.9 GHz image (Fig. 2) clearly shows that the 1.7 GHz bipolar emission exists but it is resolved out in this higher resolution image. We managed to image the extended structure of 3C 317 at 4.9 GHz, and obtained $\alpha_{1.7}^{4.9} \sim 0.77_{-0.10}^{+0.09}$.

Table 2. Parameters of the images

Band	S_{tot} mJy	S_{peak} mJy/beam	r.m.s. μ Jy/beam	Restoring FWHM and PA mas, $^{\circ}$
L	353 ± 14	276 ± 11	64	6.0×5.0 (mas) at 0°
C	345 ± 14	155 ± 6	65	2.0×1.7 (mas) at 0°
X	217 ± 9	102 ± 4	90	1.5×0.6 (mas) at 0°

The images made at 4.9 GHz and 8.3 GHz for the determination of the spectral index are detailed enough to allow an estimate of $\alpha_{4.9}^{8.3}$ in the compact component C and a global value in the northern and southern region. We found that $\alpha_{4.9}^{8.3}(C) \sim 0.7 \pm 0.2$, while we found average values of 1.2 ± 0.2 and 1.1 ± 0.2 in the northern and southern region respectively. Our analysis confirms that component C may host the “core” of the radio emission. The total spectral index was computed on the basis of the total flux density in the two images, derived by means of the task TVSTAT. We found $\alpha_{4.9}^{8.3} \sim 0.9 \pm 0.2$.

In order to get a global picture of the radio spectrum of 3C 317, from the literature we collected the total flux density measurements, the arcsecond core data (Morganti et al. 1993, Zhao et al. 1993), the milliarcsecond data (Venturi et al. 2000), and plotted them in Fig. 4 together with the total flux density data from the present work (see Table 2).

Our data are in excellent agreement with the previous observations on the parsec and on the sub–arcsecond scale. Moreover, the addition of the parsec scale 8.3 GHz flux density clearly shows the presence of a nuclear turnover ν_{to} between 1.7 and 5 GHz, ruling out the possibility of a flat spectrum from 1.7 up to 8.3 GHz. We note that the nuclear spectrum shown in Fig. 4 is considerably steep for $\nu > \nu_{to}$. The values of the spectral index obtained for the various features in the source are summarised in Table 3. We are aware of the fact that the spectral index in the bipolar emission on the scale of 20 – 40 pc is considerably flatter than in the innermost regions. It is not clear how these values can be reconciled. One possibility is that the jet flow experiences some form of reacceleration on the scale of ~ 10 pc. Under this hypothesis, the lack of emission beyond this distance in the 4.9 GHz image would then be due to an increase in the jet transport efficiency, rather than to a surface brightness decrease as consequence of jet broadening. Alternatively, small oscillations of the symmetric jet structure in the direction of the line of sight may influence our total flux density measurements, thus affecting the estimate of the spectral index. Unfortunately, our data and images are not adequate to investigate any of these suggestions.

4.2. Analysis of the parsec scale spectrum

We carried out a detailed study of the total parsec scale spectrum of 3C 317, in order to derive an estimate of the break frequency ν_{br} and of the injection spectrum of the radiating electrons. We used the most updated version of

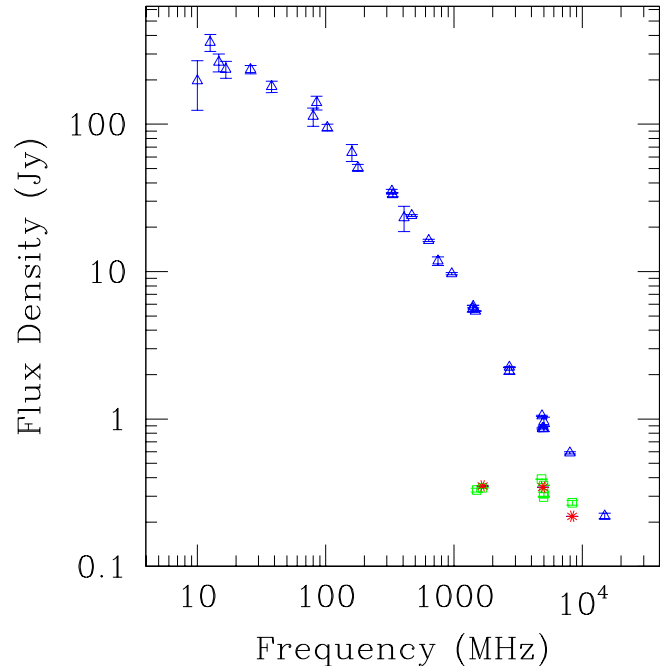


Fig. 4. Spectrum of 3C317 from 10 MHz to 15 GHz. Red stars represent the VLBA data presented in this paper; open blue triangles refer to the total flux density measurements from the literature, open green squares are core flux density derived in previous works (see Venturi et al. 2000 for references).

Table 3. Spectral index of the components of the milliarcsecond structure of 3C 317

	$\alpha_{1.7}^{4.9}$	$\alpha_{4.9}^{8.3}$
Central component	-0.01	+0.9
Bipolar emission	+0.77	-
Component C	-	+0.7
Region N	-	+1.2
Region S	-	+1.1

the program Synage (Murgia & Fanti 1996), and found that the best fit to our spectrum is given by a “continuous injection” model (Kardashev 1962), with an initial electron injection index $\alpha_{inj} = 0.55$, a break frequency $\nu_{br} \sim 6.5$ GHz and a turnover frequency $\nu_{to} \sim 2.6$ GHz

(see Fig. 5). We note that the flux density values used for the best fit refer to the inner 10 mas of 3C317, i.e. the bipolar emission at 1.7 GHz is not included.

4.3. The physical conditions at equipartition

In order to understand the nature of 3C317 and compare its parsec-scale properties to those of other classes of compact radio sources, for each component (see Fig. 3) we computed the intrinsic parameters in the source, i.e. magnetic field, internal pressure and total energy, assuming that equipartition holds in the source.

We used the standard formulae in Pacholczyk (1970), assuming that the relativistic particles and the magnetic field fully occupy the same volume ($\Phi = 1$), and that the amount of energy in heavy particles is the same as that in electrons ($k = 1$). We integrated over the frequency range $10^7 - 10^{11}$ Hz, used an ellipsoidal geometry for each component and the values for ν_{br} and α_{inj} derived from the study of the nuclear spectrum.

For the nuclear region imaged at 8.3 GHz (component C, and the two short twisted jets) we obtained a global equipartition magnetic field $H_{eq} \sim 4.3 \times 10^{-2}$ Gauss, while in the extended bipolar emission detected at 1.7 GHz we found an average value $H_{eq} \sim 2.4 \times 10^{-3}$ G. The total energy is $E_{tot} \sim 9.5 \times 10^{51}$ and $\sim 3 \times 10^{52}$ erg for the central region and for the bipolar emission respectively. The corresponding minimum internal pressures are $P_{eq} \sim 1.7 \times 10^{-5}$ and $\sim 2 \times 10^{-7}$ dyn/cm².

4.4. Considerations from the spectral analysis

The nuclear properties of 3C317, as derived from our spectral analysis, are similar to those found in Compact Steep Spectrum sources (CSS).

The spectrum of the nuclear region in 3C317, with a turnover at $\nu_{to} \sim 2.6$ GHz, and the steep spectrum for $\nu > \nu_{to}$ are reminiscent of the spectra of Giga-Hertz Peaked-Spectrum (GPS) radio sources, as it can be clearly seen in O’Dea (1998) and in Stanghellini et al. (1998). Moreover, other properties of the source show similarities with CSS and GPS sources. Beyond the double sided emission on the nuclear scale, the lack of polarisation is consistent with the finding in Cotton et al. (2003) and Fanti et al. (2004) for a sample of CSS radio sources: intrinsically small radio sources appear to be unpolarised on scales smaller than a few kpc, and the projected linear size at which the sources start to be statistically polarised gets smaller with increasing frequency (Fanti et al. 2004). In particular, the projected linear size (10 pc) of the structure in Fig. 3 requires no polarisation at X band, as observed. In summary, as it is the case for most of the CSS sources unpolarised on the VLA scales, beam depolarisation is not effective.

Last but not least, our estimates for the equipartition parameters are in good agreement with the values found for other compact sources with comparable size and ra-

dio power. The equipartition field values H_{eq} found from VLBA observations of the compact steep spectrum sources in the B3-VLA sample go up to 20 mG (Dallacasa et al. 2002), and their average value is of the order of 2 mG, as found in the 1.7 GHz bipolar emission of 3C317.

5. Discussion

The results of our multifrequency parsec-scale study of 3C317 can be briefly summarised as follows.

(a) The source has a two-sided morphology, whose overall position angle rotates by $\sim 20^\circ - 25^\circ$ going from a few mas (8.3 GHz) out to a few tens of mas (1.7 GHz). At 8.3 GHz 3C317 is characterised by a central component and two short symmetric jets, ending into two high brightness regions, with a twisted S-shaped morphology. In the following discussion we will refer to these two regions as to the *lobes*. Constraints from the flux density asymmetry suggest that 3C317 lies almost in the plane of the sky, i.e. it is viewed under an angle $\theta \sim 81^\circ - 85^\circ$;

(b) the total spectrum on the parsec scale is convex, with a turnover $\nu_{to} \sim 2.6$ GHz, and a steep spectral index at frequencies $\nu > \nu_{to}$, i.e. $\alpha_{4.9}^{8.3} \sim 0.9$;

(c) the source is unpolarised on this scale, and the magnetic field is randomly oriented;

(d) the average magnetic field at equipartition in the nuclear region and in the extended bipolar emission (1.7 GHz image at the resolution 6×5 mas) is respectively $H_{eq} \sim 43$ mG and 2.4 mG. These values, and the other equipartition parameters, are in agreement with those found for GPS sources and for the most compact CSS sources.

The S-shaped morphology of 3C317 at high resolution is reminiscent of 1946+708 (Taylor & Vermeulen 1997) and 2352+495 (Wilkinson et al. 1994), classified as Compact Symetric Objects (CSOs, see O’Dea 1998 for a recent review). This feature, together with points (b), (c) and (d) above, suggest that the nuclear region of 3C317 itself may be a member of this class.

5.1. Restarted activity in the nucleus of 3C317?

It is now accepted that CSO radio sources are on average young objects, which will evolve into sources of large angular size, either FRI or FRII radio galaxies, depending on the initial radio power (Fanti et al. 1995; Readhead et al. 1996; Owsianik & Conway 1998). In particular, the detection of hotspot proper motion in ~ 12 CSOs (Polatidis et al. 2002; Polatidis & Conway 2003), coupled with recent “spectral ageing” studies (Murgia 2003), strongly support the proposed evolutionary scenario.

In order to test the suggestion that the nucleus of 3C317 is a CSO, we computed the equipartition field H_{eq} in the lobes N and S of the high resolution 8.3 GHz image and used the formula by Murgia (2003) to estimate the radiative age of the electrons in these regions (see Fig. 3):

$$t_{syn}(yr) = 5.03 \times 10^4 \times (H_{eq})^{-3/2} [(1+z)\nu_{br}]^{-1/2}$$

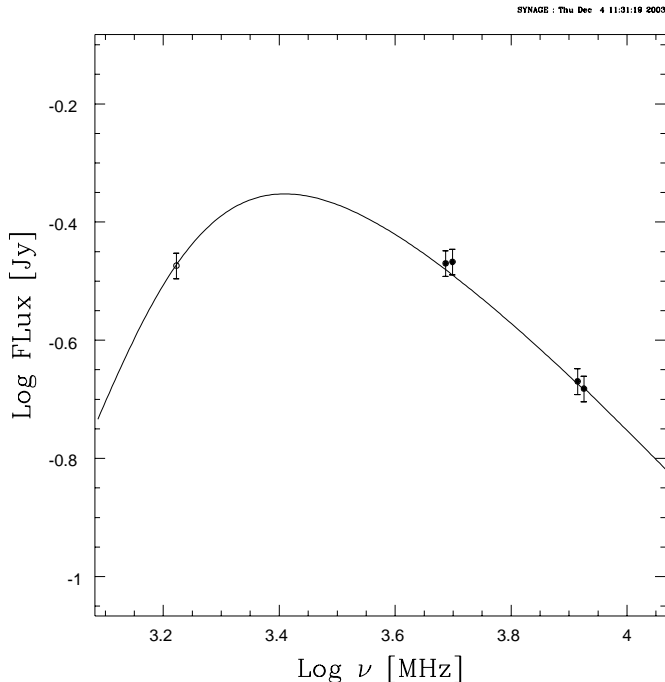


Fig. 5. Best fit of the nuclear spectrum of 3C 317 obtained with the program Synage using a “continuous injection” model.

where H_{eq} is in units of mG and ν_{br} in GHz. We could not carry out a detailed spectral study for the lobes, given the very small number of resolution elements along the structure, therefore we assumed an upper limit for ν_{br} of the order of 6.5 GHz, i.e. the break frequency for the whole nuclear region (see Section 4.3). We estimated an equipartition field of 23.5 mG, and derived an average radiative age for the two lobes of the order $t_{syn} = 170$ yr. This result suggests that the radio emission coming from the nuclear region very is young.

We used the radiative age to estimate the expected proper motion in the inner region of 3C 317. Murgia (2003) showed that the radiative (t_{syn}) and dynamic age (t_{dyn}) are in very good agreement in the only well studied case, i.e. B 1943+546, so our approach is based on this result. Assuming $t_{syn} = t_{dyn} = 170$ yr, and a distance of ~ 7 pc between the two lobes (see Fig. 3), we obtained a separation velocity $v_{sep} \sim 0.14 hc$. This value is in the range of proper motions found in the hot spots of CSOs reported in Polatidis & Conway (2003).

The very young dynamical and radiative ages of CSOs poses the problem of recurrent activity. Beyond the theoretical work of Reynolds & Begelman (1997), hints on the fact that the life of a radio source may be characterized by alternate active and quiescent phases come from a number of observational results. In particular, (a) the

large angular size double–double radio galaxies (DDRGs) are interpreted as due to intermittent radio activity in the host galaxy (Schoenmakers et al. 2000; Lara et al. 1999); (b) the existence of a superluminal parsec–scale nucleus associated with an old extended radio galaxy has been found in B2 1144+35 (Giovannini et al. 1999) and in 3C 338 (Giovannini et al. 1998), pointing again in the direction of restarted radio activity; (c) finally, recurrent activity in central dominant cluster galaxies is suggested by the correlation between X–ray cavities and low brightness radio emission in galaxy clusters (McNamara et al. 2000).

In the case of CSOs, assuming that even a fraction of them represents a renewed cycle of radio activity, old extended radio emission should be found around some members of this class. This is indeed the case for a few objects, such as 0108+388 (Owsianik et al. 1998), 0402+379 (Maness et al. 2003) and 1245+676 (Marecki et al. 2003).

The nuclear properties of 3C 317, coupled with the information on the arcsecond scale radio emission, and the high resolution X–ray Chandra images of the intracluster gas in A 2052, are consistent with the idea that the radio activity in 3C 317 is recurrent, and that at present the source is undergoing a newly born active cycle.

We estimated the age of the bipolar radio emission over ~ 40 pc, well visible at 1.7 GHz and detected also at 4.9 GHz. We note that we have no information on the break frequency ν_{br} for this feature. Given our knowledge on the inner CSO structure, we assumed that $\nu_{br} < 5$ GHz, and derived that the radiative age must be $t_{syn} > 6 \times 10^3$ yr. Even though we should consider this result only as indicative, due to the underlying assumptions on the break frequency, we note that this lower limit is in reasonable agreement with the hypothesis made by many authors that the duration of the cycles of activity is in the range $10^4 - 10^5$ yr (i.e. Reynolds & Begelman 1997).

In order to complete our study of the radio emission age in 3C 317, we fitted the spectrum of the extended arcsecond emission, in order to derive the overall source age. The best fit to the spectrum is given by a continuous injection model with self–synchrotron absorption, and provides a break frequency $\nu_{br} = 780$ MHz. We wish to point out that the continuous injection model does not contradict the proposed frame of recurrent activity, since during the lifetime of the extended radio emission the nucleus appears “on average” active. If we assume an average magnetic field of $\sim 20 \mu\text{G}$ (Zhao et al. 1993) we obtain a global age $t_{syn} \sim 2 \times 10^7$ yr.

5.2. Alternative interpretations

5.2.1. Slow jets?

An alternative hypothesis to recurrent bursts of radio activity in 3C 317 is the possibility that the intrinsic plasma speed in the jets is not relativistic, and that major interaction with the external medium prevents them from a full development. Our high frequency and high resolu-

tion images clearly show that no trace of collimated jets is visible beyond ~ 10 mas from the peak. The symmetry of the parsec-scale emission (as discussed in Section 3.1) suggests that relativistic beaming is playing a small role for this source, therefore mild intrinsic speeds are not contradicted by our results.

However, we know from the arcsecond emission that the plasma indeed reaches those scales, therefore relatively fresh electrons must be transported out on scales of tens of kpc, given that buoyancy is not effective to produce such extended emission on timescales of the order of 10^7 years.

5.2.2. Particle reacceleration in the cooling flow

Another intriguing possibility is that the extended radio emission in 3C 317 is a *mini-halo*. Such radio sources are found around powerful radio galaxies located at the centre of cooling core clusters. Observationally, their extension is of the order of a few hundred kpc, and they are characterised by low brightness extended emission with a steep spectrum ($\alpha > 1$). The prototypical example of this class of radio sources is 3C 84 in Perseus (Burns et al. 1992). Mini-halos have been recently explained in terms of reacceleration of old relativistic electrons, due to MHD turbulence in the cooling flow (Gitti et al. 2002).

A comparison between the radio and X-ray emission in the Perseus cluster and in A2052 is providing very interesting pieces of information. The similarity of the radio/X-ray overlay in the inner region of the two clusters, i.e. within ~ 1.5 arcmin (Fabian et al. 2000 and Blanton et al. 2001, respectively for Perseus and A2052) is impressive. Furthermore, the 327 MHz overall morphology of the inner 10 arcmin in 3C 84 (Sijbring 1993) is identical to that of 3C 317 at the same frequency (Zhao et al. 1993). From this image, the largest linear size of 3C 317 is only ~ 130 kpc, to be compared respectively to the ~ 400 kpc and ~ 200 kpc of the mini-halos in Perseus and in A 2626 (Gitti et al. 2004). We note however that the high resolution of the 327 MHz image in Zhao et al. ($5'' \times 5''$) does not allow a thorough comparison. Imaging at low frequency and resolution, and high sensitivity is necessary to properly study the case of 3C 317.

We are at present investigating the possibility that the extended emission of 3C 317 is also the result of reacceleration mechanisms due to the central cooling flow.

6. Conclusions

Our polarimetric VLBA multifrequency observations of 3C 317, the central radio galaxy in the cooling core cluster A 2052, revealed a compact double morphology over a scale of few mas. The observational properties are consistent with the idea that the nucleus of 3C 317 is a young CSO. In particular, the peak in the radio spectrum at ~ 2.6 GHz, the lack of polarisation, the orientation almost in the plane of the sky, and the values of the intrinsic physical parameters are common to CSS and to GPS sources. The radiative age of the inner source

structure, estimated from our observations, is only ~ 170 yr.

Assuming that the radiative age and the dynamic age of the source are similar, we predict that the parsec-scale lobes in 3C 317 are moving away from each other at a speed $v_{sep} \sim 0.14 hc$.

On the arcsecond scale, the nucleus of 3C 317 is surrounded by an extended amorphous “halo” of low brightness radio emission, which spatially anticorrelates with the cluster X-ray emission. In particular, the radio plasma is found to fill gaps of X-ray brightness, supporting the recent suggestion that the radio plasma sweeps the thermal intracluster gas and compresses it into bright shells. An intriguing possibility is that the extended amorphous halo is the result of reacceleration processes due to MHD turbulence in the cooling flow.

The young age estimated for the radio nucleus of 3C 317, coupled with the existence of large scale radio emission, leads us to suggest that the radio galaxy is characterised by intermittent radio emission in the nucleus, and that a new phase of activity has just started. This result is relevant not only in the light of our understanding of radio source birth and evolution, but it is also an important piece of information for our knowledge of the interaction between the non thermal radio emission and the hot thermal gas in clusters of galaxies.

Acknowledgements. The authors wish to thank M. Murgia and C. Stanghellini for their insightful comments on the paper. Thanks are due to the staff of observatories who participated in these observations and the Socorro correlator staff. The National Radio Astronomy Observatory (NRAO) is operated by Associated Universities Inc., under cooperative agreement with the National Science Foundation. This research has made use of the NASA/IPAC Extragalactic Database (NED) which is operated by the Jet Propulsion Laboratory, Caltech, under contract with NASA. This research has also made use of NASA’s Astrophysics Data System Abstract Service. FS acknowledges financial support from IRA-CNR under grant N. 126.59.BO.2. DD acknowledges financial support under grant MIUR COFIN 2002-02-8118.

References

- Baum, S.A. & O’Dea, C.P., 1991, MNRAS, 250, 737
- Böhringer, H., Voges, W., Fabian, A.C., et al., 1993, MNRAS, 264, L25
- Burns, J.O., 1990, AJ, 99, 14
- Burns, J.O., Sulkanen, M.E., Gisler, G.R., et al., 1992, ApJ, 388, L49
- Blanton, E.L., Sarazin, C.L., McNamara, B.R., et al., 2001, AJ, 558, L15
- Cotton, W.D., 1993, AJ, 106, 1241
- Cotton, W.D., Dallacasa, D., Fanti, C., et al., 2003, A&A, 406, 43
- Dallacasa, D., Tinti, S., Fanti C., et al., 2002, A&A, 389, 115
- David, L.P., Nulsen, P.E.J., McNamara, B.R., et al., 2001, ApJ, 557, 546
- Fabian, A.C., Sanders, J.S., Ettori, S., et al., 2000, MNRAS, 318, L65

- Fanaroff, B.L., & Riley, J.M., 1974, MNRAS, 167, 31
- Fanti, C., Fanti, R., Dallacasa, D., et al., 1995, A&A, 302, 317
- Fanti, C., Branchesi, M., Cotton, W.D., et al., 2004, A&A, submitted
- Ge, J.P., & Owen, F.N., 1993, AJ, 105, 778
- Ge, J.P., & Owen, F.N., 1994, AJ, 108, 1523
- Giovannini, G., Cotton, W.D., Feretti, L., et al., 1998, ApJ, 493, 632
- Giovannini, G., Taylor, G.B., Arbizzani, E., et al., 1999, ApJ, 522, 101
- Gitti, M., Brunetti, G., & Setti, G., 2002, A&A, 386, 456
- Gitti, M., Brunetti, G., Feretti, L., et al., 2004, A&A, 417, 1
- Jiang, D.R., Dallacasa, D., Schilizzi, R.T., et al., 1996, A&A, 312, 380
- Kardashev, N.S., 1962, SvA, 6, 317
- Lara, L., Marquez, I., Cotton, W.D., et al., 1999, A&A, 348, 699
- Maness, H.L., Taylor, G.B., Zavala, R.T., et al., 2003, ApJ, 602, 123
- Marecki, A., Spencer, R.E., Kunert, M., 2003, PASA, 20, 46
- McNamara, B.R., Wise, M., Nulsen, P.E.J., et al., 2000, ApJ, 534, L135
- Morganti, R., Killeen, N., & Tadhunter, C.N., 1993, MNRAS, 263, 1023
- Murgia, M., & Fanti, R., 1996, Rapporto Interno IRA, 228/96
- Murgia, M., 2003, PASA, 20, 19
- O'Dea, C.P. & Baum, S.A., 1987, in *Radio Continuum Processes in Clusters of Galaxies*, NRAO Conference Proceedings, Eds. C.P. O'Dea & J.M. Uson, p. 141
- O'Dea, C.P., 1998, PASP 110, 493
- Owsianik, I., & Conway, J.E., 1998, A&A, 337, 69
- Owsianik, I., Conway, J.E., & Polatidis, A.G., 1998, A&A, 336, L37
- Pacholczyk, A.G., 1970, Radio Astrophysics (San Francisco: Freeman & Co.)
- Polatidis, A.G., & Conway, J.E., 2003, PASA, 20, 69
- Polatidis, A.G., Conway, J.E., & Owsianik, I., 2002, Proceedings of the 6th European VLBI Network Symposium, Eds. E. Ros, R.W. Porcas, A.P. Lobanov & J.A. Zensus, p. 139
- Readhead, A.C.S., Taylor, G.B., Pearson T.J., et al., 1996, ApJ, 460, 634
- Reynolds, C.S., & Begelman, M.C., 1997, ApJ, 487, L135
- Rizza, E., Loken, C., Bliton, M., et al., 2000, AJ, 119, 21
- Sarazin, C.L., Baum, S.A., & O'Dea, P.N., 1995, ApJ, 451, 125
- Schoenmakers, A.P., de Bruyn, A.G., Röttgering, H.J.A., et al., 2000, MNRAS, 315, 371
- Sijbring, D., 1993, Ph. D. Thesis, Groningen
- Stanghellini, C., O'Dea, C.P., Dallacasa, D., et al., 1998, A&A, 131, 303
- Taylor, G.B., Inoue, M., & Tabara H., 1992, A&A, 264, 421
- Taylor, G.B., & Perley, R.A., 1993, ApJ, 416, 554
- Taylor, G.B., Barton, E.J., & Ge, J., 1994, AJ, 107, 1942
- Taylor, G.B., & Vermeulen, R.C., 1997, ApJ, 485, L9
- Venturi, T., Morganti, R., Tzioumis T., et al., 2000, A&A, 363, 84
- Wilkinson, P.N., Polatidis, A.G., Readhead, A.C.S., et al., 1994, ApJ, 432, L87
- Zhao, J.H., Sumi, D.M., Burns, J.O., et al., 1993, ApJ, 416, 51